

# Fourier Neural Operators for Learning Dynamics in Quantum Spin Systems

Freya Shah,<sup>1,2</sup> Taylor L. Patti,<sup>3</sup> Julius Berner,<sup>1</sup> Bahareh Tolooshams,<sup>1</sup> Jean Kossaifi,<sup>3</sup> and Anima Anandkumar<sup>1</sup>

<sup>1</sup>*Department of Computing + Mathematical Sciences (CMS),  
California Institute of Technology (Caltech), Pasadena, CA 91125, USA*

<sup>2</sup>*Ahmedabad University, Ahmedabad 380015, Gujarat, India*

<sup>3</sup>*NVIDIA, Santa Clara, CA 95051, USA*

Fourier Neural Operators (FNOs) excel on tasks using functional data, such as those originating from partial differential equations. Such characteristics render them an effective approach for simulating the time evolution of quantum wavefunctions, which is a computationally challenging, yet coveted task for understanding quantum systems. In this manuscript, we use FNOs to model the evolution of random quantum spin systems, so chosen due to their representative quantum dynamics and minimal symmetry. We explore two distinct FNO architectures and examine their performance for learning and predicting time evolution using both random and low-energy input states. Additionally, we apply FNOs to a compact set of Hamiltonian observables ( $\sim \text{poly}(n)$ ) instead of the entire  $2^n$  quantum wavefunction, which greatly reduces the size of our inputs and outputs and, consequently, the requisite dimensions of the resulting FNOs. Moreover, this Hamiltonian observable-based method demonstrates that FNOs can effectively distill information from high-dimensional spaces into lower-dimensional spaces. The extrapolation of Hamiltonian observables to times later than those used in training is of particular interest, as this stands to fundamentally increase the simulatability of quantum systems past both the coherence times of contemporary quantum architectures and the circuit-depths of tractable tensor networks.

Simulating the dynamics of quantum systems has been a long-standing goal for the scientific community, underpinning Feynman’s initial proposition of quantum computing [1–3]. Learning and predicting the behavior of intricate quantum spin systems presents a significant challenge due to their inherent superpolynomial time complexity [4]. Controllable quantum systems, such as quantum simulators or other quantum computers, represent a promising pathway for simulating complex quantum systems, as they share similar dynamics and large Hilbert spaces [5–10]. However, current quantum computing technologies face significant limitations [11]. In the present Noisy Intermediate-Scale Quantum (NISQ) era, quantum computers are restricted to a limited number of qubits and substantial error rates due to decoherence and operational imperfections [12, 13]. These coherence and scalability issues constrain the capacity of quantum computers to simulate large and complicated spin systems, particularly over long timescales. As a result, achieving substantial and accurate results in the simulation of these systems remains elusive.

Advances in quantum modeling have introduced promising new approaches for quantum simulation, addressing limitations of traditional techniques. For instance, tensor methods like the Density Matrix Renormalization Group (DMRG) are capable of simulating larger quantum systems [14–17]. Tensor methods are highly effective for certain applications, such as studying ground state properties in one-dimensional systems but they encounter significant limitations when extended to systems with higher dimensions or greater levels of entanglement. Likewise, machine learning techniques based on neural networks, such as Neural-Network Quantum States (NQS) and Heisenberg Neural Networks (HENN), capture the essence of large quantum systems

with a smaller-dimensional model. NQS provides a compact representation of many-body quantum states with artificial neural networks, capturing intrinsically non-local correlations and improving scalability over conventional approaches [18–21], while HENN reconstructs time-dependent quantum Hamiltonians from local measurements, employing a physics-informed loss function based on the Heisenberg equation of motion and achieving high tomographic fidelity with sparse data [22, 23]. However, such machine learning-based approaches have marked limitations in accuracy, particularly when they model large quantum systems and long evolution times.

Moreover, traditional neural networks struggle with generalizing across different discretizations, often requiring re-training or adjustments to maintain accuracy when applied to new discretization schemes. In contrast, Fourier Neural Operators (FNOs) provide a compelling alternative by learning operators between infinite-dimensional function spaces, leveraging their resolution-invariance [24–29]. This allows FNOs to be trained at lower resolutions and seamlessly perform evaluations at higher resolutions, a phenomenon known as zero-shot super-resolution. Moreover, FNOs maintain consistent error rates across varying resolutions and offer exceptional computational efficiency, performing orders of magnitude faster than traditional solvers for partial differential equations (PDEs) [24, 30–33]. Recent studies demonstrate the effectiveness of FNOs in representing the S-matrix and solving fundamental quantum problems, such as the double-slit experiment and wave packet scattering [34]. However, the study primarily focuses on relatively simple quantum problems, which, while illustrative, have limited practical application.

**Our approach:** We explore whether FNOs can effectively learn the dynamics of quantum wavefunctions

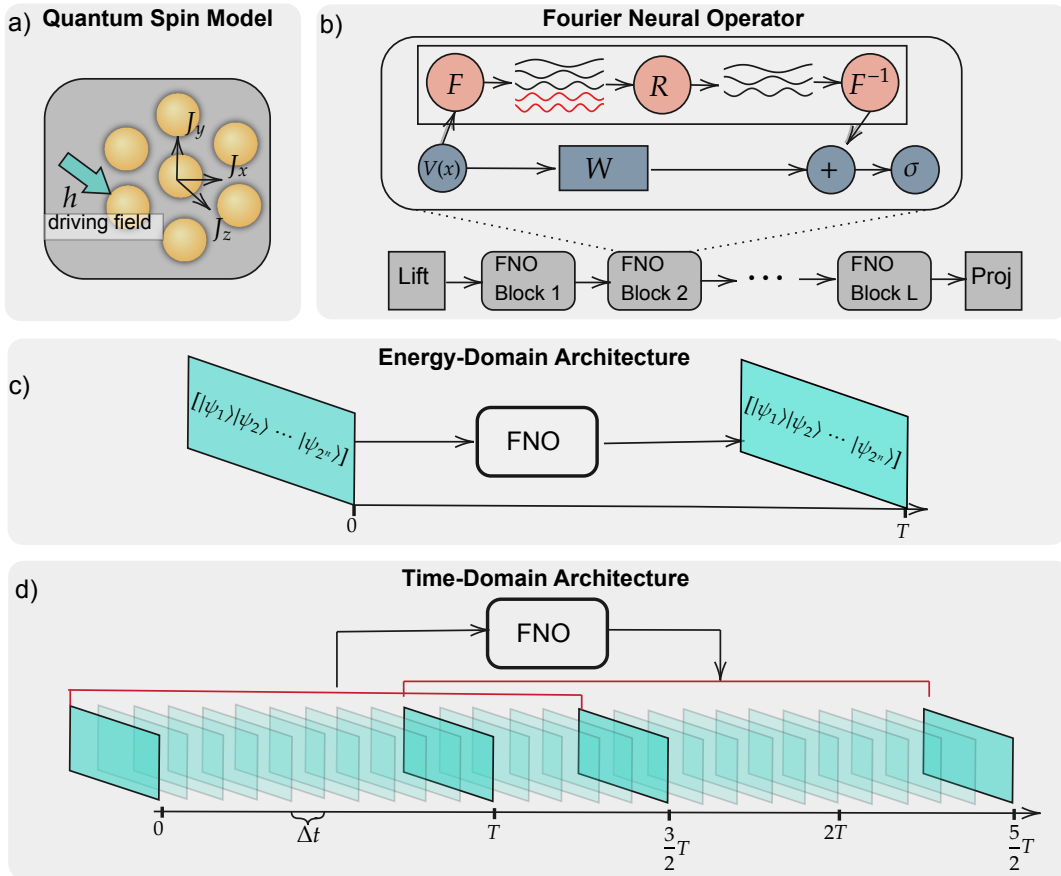


Figure 1: **(a)** Schematic representation of quantum spin system used to model its dynamics using FNOs, where  $J_x$ ,  $J_y$ , and  $J_z$  represent the coupling constants and  $h$  denotes the external driving field. **(b)** Diagram illustrating the FNO framework, which consists of multiple FNO blocks performing spectral convolution over the input in the latent space. **(c)** We investigate two distinct architectures for learning dynamics in quantum spin systems. The first is the energy-domain architecture (see Section IB 1), where the input is the wavefunction at the initial time  $t = 0$ , and the output is the wavefunction evolved to time  $t = T$ . **(d)** The second is the time-domain architecture (see Section IB 2), which takes the wavefunction evolved over the initial time interval  $[0, \frac{3}{2}T]$  (discretized on a grid with width  $\Delta t$ ) as input and produces an output wavefunction over the time interval  $[T, \frac{5}{2}T]$ .

in quantum systems, such as quantum spin systems [35]. Given the limitations of contemporary quantum simulators, FNOs present a potential tool for studying quantum systems, learning their dynamics and, most interestingly, extrapolating those dynamics to timescales that are not possible either experimentally (due to coherence times) or computationally (due to, e.g., the growing rank of tensor networks with increased circuit-depth or time-evolution). As quantum dynamics are dictated by the Schrödinger equation, which is a PDE of the FNOs for learning the time-evolution operator is well motivated. We employ temporal data from actual quantum computations to train FNOs, enabling them to capture system dynamics, extrapolate future time intervals, and generate predictions for analogous inputs. This methodology has the potential to address the limitations imposed by quantum decoherence, which impedes large-scale and prolonged simulations.

The time-evolution of spin systems is particularly advantageous for exploring the application of FNOs, as they are fundamental models that encapsulate a wide array of complex phenomena inherent in quantum mechanics [36]. These simplified systems are instrumental in elucidating various quantum many-body effects, such as quantum phase transitions, gauge symmetries, and spin liquids, while also facilitating the discovery of novel, uncharacterized phenomena [37]. Notable examples of these models include the Ising model, the Heisenberg model, and the XY model. The large-scale simulation of these spin systems is of paramount importance due to their extensive applications in fields such as condensed matter physics, high-energy particle physics, and quantum gravity [37].

In this manuscript, we numerically demonstrate the effectiveness of FNOs in learning the time evolution operator for the wavefunction of an 8-qubit Heisenberg 1D chain with random single-qubit driving. Two distinct

FNO architectures are designed: the energy-domain architecture and the time-domain architecture. Moreover, we illustrate the model’s ability to extrapolate dynamics to future time intervals with minimal error rates.

In addition to using these two architectures on the full quantum wavefunction, we also deploy the time-domain architecture using a mere polynomial number of Hamiltonian observables as inputs and outputs. We are motivated to study this compact architecture because the full wavefunction analyses have utility only at scales for which classical simulations can provide a ground-truth calculation. Conversely, the more compact Hamiltonian observable training procedure can be applied to data from quantum devices that exceed the capabilities of classical simulations, representing a powerful future goal. This could enable the study of quantum systems that are too large to simulate classically on timescales that are too long to carry out experimentally. Another advantage of using Hamiltonian observables as inputs is that this can push the boundaries of tensor network simulation beyond what computationally-tractable bond dimensions, which increase linearly with the number of qubits but grow exponentially with circuit or unitary depth, can allow. This is because an FNO can be trained on data from shallower tensor networks and then be used to extrapolate to longer timescales, whereas simulating the same system directly with a deeper tensor network would result in computationally prohibitive bond dimensions. To demonstrate the potential of this goal, we extrapolate the dynamics of these Hamiltonian observables into timescales longer than those provided by the training data. This includes extending the Hamiltonian observable time horizon up to twice the duration of the training period, with a relative error of just 6.46%.

In the time-domain architecture, we achieve a substantial  $6.71\times$  speedup with FNOs compared to exact unitary evolution for inferring dynamics at later times for 8 qubit systems with only a minimal fidelity reduction of 0.04%. We note that this speedup is likely to become more substantial at larger system sizes, as both exact unitary integration and approximate integration techniques become more computationally intensive. Additionally, we demonstrate FNO’s capability for zero-shot super-resolution on 4 qubits by making predictions on a grid 10 times finer than that of the training interval. Due to its discretization-invariance, the FNO maintains exceptional accuracy, with error rates as low as 0.04% on the finer grid, while the U-Net shows a significantly increased error rate of 51.70% on the finer discretization. These results highlight FNO’s superior performance in both computational efficiency and accuracy, emphasizing its potential as a powerful tool for predicting quantum dynamics.

## I. RESULTS

### A. Preliminaries

In this section, we provide a brief overview of the quantum spin systems studied and outline the functionality of FNOs.

#### 1. Spin System Model

Quantum spin systems are characterized by two-level particles organized in a specific geometry [36, 37]. The Hamiltonian involves the interaction between neighboring quantum spins and external fields. We consider a spin  $1/2$  1D Heisenberg chain. The corresponding Hamiltonian is given by

$$H = \sum_{i=1}^n (J_z \sigma_i^z \sigma_{i+1}^z + J_x \sigma_i^x \sigma_{i+1}^x + J_y \sigma_i^y \sigma_{i+1}^y) + h \sigma_i^z, \quad (1)$$

where  $n$  represents the total number of qubits or atoms in the system. The Pauli matrix  $\sigma_i^a$ , where  $a \in x, y, z$ , is defined as  $\sigma_i^a = I^{\otimes i-1} \otimes \sigma^a \otimes I^{\otimes n-i}$ . Here,  $I$  is the  $2 \times 2$  identity matrix and  $\sigma^a$  denotes the corresponding  $2 \times 2$  Pauli matrix. The parameters  $J_x$ ,  $J_y$ , and  $J_z$  are the coupling constants for two-qubit spin interactions, while  $h$  denotes the single-qubit driving field acting along the  $z$ -direction. We restrict interactions to nearest neighbors and apply periodic boundary conditions, such that  $\sigma_{n+1}^a \equiv \sigma_1^a$ . For our analysis, we use a Hamiltonian with randomly assigned coupling constants and a single-qubit driving field, where the values are uniformly distributed in the range from  $-2$  to  $2$ . Additionally, we consider the quantum Ising Hamiltonian defined as

$$H = \sum_{i=1}^n J_z (\sigma_i^z \sigma_{i+1}^z) + h \sigma_i^x. \quad (2)$$

This Hamiltonian also involves nearest-neighbor interactions and periodic boundary conditions, along with randomly assigned  $J_z$  and  $h$ .

#### 2. Fourier Neural Operators

Neural Operators (NOs) are a class of machine learning models designed to learn mappings between infinite-dimensional function spaces, making them well-suited for a variety of applications, including ordinary differential equations (ODEs) and PDEs [38–41]. A key advantage of NOs is their resolution-agnostic nature; they can be trained on data at one resolution and generalize to different resolutions without requiring retraining. Among Neural Operators, FNOs represent a specific implementation where spectral convolutions are utilized to capture the underlying patterns in the data [24].

As shown in Figure 1 b), an FNO consists of  $L$  FNO blocks  $F_\ell$ , a lifting layer Lift, and a projection layer Proj of the form

$$\mathbf{I} \xrightarrow{\text{Lift}} \mathbf{V}_0 \xrightarrow{F_1} \mathbf{V}_1 \xrightarrow{F_2} \dots \xrightarrow{F_{L-1}} \mathbf{V}_{L-1} \xrightarrow{F_L} \mathbf{V}_L \xrightarrow{\text{Proj}} \mathbf{O}.$$

The lifting layer Lift maps the input data  $\mathbf{I}$  with a given number of input channels to a latent function  $\mathbf{V}_0$  with a (typically) larger number of channels. Here, channels denote the dimensions of the co-domain of the functions  $\mathbf{V}_\ell$ , representing distinct components or features within the latent space. The latent space is an intermediate representation where the data is abstracted into a higher-level form, capturing essential patterns and relationships. The FNO operates within this latent space by applying spectral convolutions.

Specifically, the latent dimension representation  $\mathbf{V}_{\ell+1}$  is defined as

$$\mathbf{V}_{\ell+1}(\vec{x}) = F_\ell(\mathbf{V}_\ell)(\vec{x}) = \sigma(W_t \mathbf{V}_\ell(\vec{x}) + (K_\ell \mathbf{V}_\ell)(\vec{x})), \quad (3)$$

where  $W_\ell$  is a learnable affine-linear map applied across the channels of  $\mathbf{V}_\ell$ , and  $\sigma$  is a non-linear activation function. The spectral convolution  $K_\ell$  can be defined as follows,

$$K_t \mathbf{V}_\ell = \mathcal{F}^{-1}(R_\ell \cdot \mathcal{F}(\mathbf{V}_\ell)), \quad (4)$$

where  $\mathcal{F}$  and  $\mathcal{F}^{-1}$  denote the Fourier and inverse Fourier transforms, respectively. In the Fourier domain, higher frequency modes are truncated, leaving a fixed number of lower modes that are multiplied with learnable parameters  $R_\ell$ . By combining the power of linear transformations, spectral convolutions, and nonlinear activation functions, the FNO can approximate highly non-linear operators [42].

After processing through multiple FNO blocks  $F_\ell$ , the projection layer Proj maps the latent representation to the output data  $\mathbf{O}$ , which may have one or more channels, depending on the specific architecture used as described in Sections IB 1 and IB 2.

## B. Learning Dynamics using Complete $2^n$ Wavefunction

In this approach, the full state space of a quantum wavefunction is used as input, with two distinct types of wavefunctions considered. The first type consists of complex-valued normalized wavefunctions for  $n$  particles, randomly generated from a uniform distribution between  $-1$  and  $1$ . For the second type, we uniformly distribute the wavefunction over low-energy states while setting the high-energy states to zero. This distinction is insightful, as in many physical applications, e.g., quantum chemistry [43], often only low-energy components of wavefunctions are occupied. In the remainder of this manuscript, we refer to the first input type as “random input” and

the latter as “low-energy input”. We develop two distinct FNO architectures for processing wavefunction inputs: the energy-domain and time-domain architectures, which are described in detail below. Notably, because quantum wavefunctions are complex quantities, we use a complex version of the FNO [44].

### 1. Energy-domain Architecture

We first consider the energy-domain architecture, where the Fourier transform is applied to the basis states of the wavefunction. This architecture requires a careful ordering of the wavefunction, specifically by arranging the basis states in order of increasing energy levels, so that states with lower energies precede those with higher energies. The method is described in detail in Section III. In the Fourier domain, the FNO truncates fast (high-frequency) energy transitions. In quantum physics, energy  $E$  and frequency  $\nu$  are directly related by the Planck-Einstein relation  $E = h\nu$ , where  $h$  is the Planck’s constant. Therefore, performing a Fourier transform over energy is effectively the same as performing it over frequency.

In this architecture, the input comprises various training data of the quantum wavefunction at an initial time, as shown in Figure 1 c). The input to the FNO is structured as follows

$$\mathbf{I} = [\text{Embed}_{\text{state}}, S_0] \in \mathbb{C}^{2 \times 2^n}. \quad (5)$$

The term  $S_0$  corresponds to the basis states  $S$  of a  $2^n$  wavefunction,  $[|\psi_1\rangle, |\psi_2\rangle, \dots, |\psi_{2^n}\rangle]$ , at the initial time  $t = 0$ . To enhance the learning process, we incorporate a position embedding  $\text{Embed}_{\text{state}}(k) = k/2^n$  into the input channel dimension, where  $k$  is the index associated with each basis state. This approach helps the model better understand the relationship between the states and their corresponding energy levels. The output tensor is given by

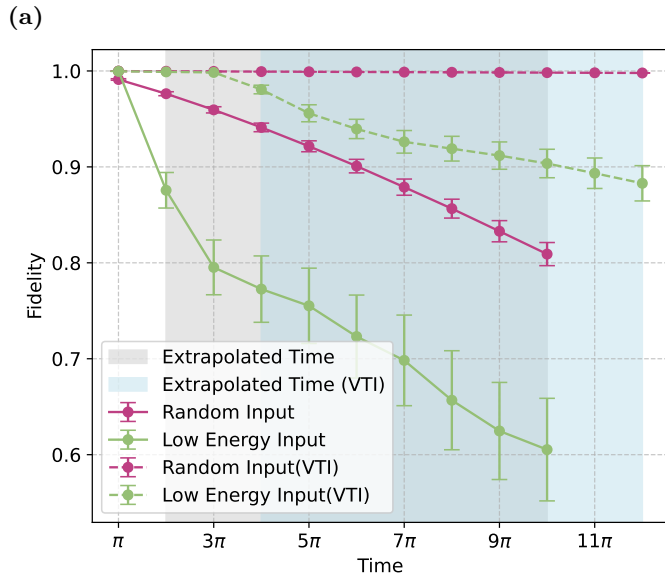
$$\mathbf{O} = S_T \in \mathbb{C}^{2^n}. \quad (6)$$

Thus the output, consists of wavefunction output evolved at  $t = T$ . In our experiments, we choose  $T = \pi$  as it represents a significant portion of the quasi-periodicity of the unitary evolution generated by the Hamiltonian  $H$ . The Fourier transform on the basis states  $S$  of the wavefunction is given by

$$\frac{1}{2^n} \sum_{k=0}^{2^n-1} \psi_k e^{\frac{-ik\tau}{\hbar}}, \quad (7)$$

Here,  $\psi_k$  is the basis state,  $\tau$  can be understood as a time-like variable, and  $\hbar$  is the reduced Planck constant. By truncating the transformed modes, we effectively filter out the components where energy values change rapidly, thus eliminating fast transitions. By concentrating on the slow-transition dynamics, the FNO highlights the most

relevant dynamics of the quantum system. While this architecture provides a physical interpretation as a Fourier transform along the wavefunction’s energy space, it does not support further discretization of the time interval  $[0, T]$ , thereby limiting its utility in scenarios requiring more fine-grained prediction of the time-evolution. We will address this issue with our time-domain architecture in Section IB 2.



(b)

n	Input	Fidelity $[0, \pi]$	Fidelity $[2\pi, 10\pi]$
4	Random	$0.9983 \pm 0.0$	$0.9732 \pm 2.3e-02$
8	Random	$0.9920 \pm 0.0$	$0.9062 \pm 5.8e-02$

n	Input	Fidelity $[0, 3\pi]$	Fidelity $[4\pi, 12\pi]$
4	Low Energy (VTI)	$0.9999 \pm 0.0$	$0.9992 \pm 1.0e-03$
8	Low Energy (VTI)	$0.9996 \pm 0.0$	$0.9430 \pm 4.2e-02$

Figure 2: **(a)** Prediction of temporal dynamics in an 8-qubit Heisenberg spin system using the energy-domain architecture in Section IB 1. At time  $T = \pi$ , the predictions made by the FNO are on unseen data but still within the time range it was trained on. The extrapolated time refers to future time predictions beyond the range on which the FNO was trained. VTI (Various Time Interval) indicates training on multiple time intervals, i.e.,  $[0, T]$ ,  $[T, 2T]$ , and  $[2T, 3T]$ , instead of training only on the first interval. **(b)** The results show the mean fidelity for time intervals the FNO has seen during training and extrapolated time intervals for systems with 4 and 8 qubits.

We use fidelity as the primary metric to evaluate the performance of the FNO in predicting quantum wavefunction dynamics. Fidelity measures the similarity between two quantum states and is defined as,

$$F(\psi_{\text{true}}, \psi_{\text{pred}}) = |\langle \psi_{\text{true}} | \psi_{\text{pred}} \rangle|^2, \quad (8)$$

where  $\langle \psi_{\text{true}} | \psi_{\text{pred}} \rangle$  is the inner product between the true and predicted wavefunctions. Additionally, we iteratively apply the model to its own predictions to forecast wavefunction dynamics over a period of up to  $t = 10T$ . Although the model is trained on the time interval  $[0, T]$ , this iterative approach allows it to predict wavefunction evolution well beyond the training data time-horizon.

Experiments are conducted using 4 and 8 qubits with both random and low-energy input states. For low-energy states, training is conducted over various time intervals (VTI), such as  $[0, T]$ ,  $[T, 2T]$ , and  $[2T, 3T]$ , rather than relying on a single time interval  $[0, T]$ . Utilizing multiple time intervals is crucial to generalize to future time intervals for low-energy states. Specifically, when training on only a single time step, the model fails to adequately capture the dynamics necessary for accurate future time predictions, despite showing strong performance during training. This is seen in Figure 2, where 8-qubit with low energy states has a mean fidelity of 0.7538 for prediction of future time until  $t = 10T$  despite achieving a fidelity of 0.9998 during training. This discrepancy underscores the importance of multi-step training for low-energy states, as these states initially occupy only low-energy configurations and gradually transition to higher-energy states over time. We test VTI when training models on random inputs. However, random inputs do not need to be trained across multiple intervals, as they already occupy a wide array of energy regions and can thus successfully extrapolate to later times with a fidelity greater than 94%. Figure 2 demonstrates that the model achieves high fidelity for both input types and can accurately predict future states while maintaining consistent fidelity across these predictions.

## 2. Time-domain Architecture

An alternative architecture involves predicting the evolution of the wavefunction on a whole time interval instead of a single time  $T$ . In practice, we need to discretize the time interval. However, using a discretization-agnostic model, such as an FNO, we train and predict using grids with arbitrary width  $\Delta t$ . Instead of a single time  $t = 0$ , we then use a time interval as input, i.e.,

$$\mathbf{I} = [\text{Embed}_{\text{time}}, S_{[0, \frac{3}{2}T]}] \in \mathbb{C}^{(2^n + 2) \times m}, \quad (9)$$

where  $m = \frac{3}{2}T/\Delta t$  defines the number of equidistant time-steps in the interval  $[0, \frac{3}{2}T]$ . For training, we choose  $T = \pi$  and  $\Delta t = \pi/10$ . For the positional embedding  $\text{Embed}_{\text{time}}$ , we use the values of two sinusoidal functions applied to the time-grid in order to assist the FNO in learning temporal patterns. The output of the FNO is given as

$$\mathbf{O} = S_{[T, \frac{5}{2}T]} \in \mathbb{C}^{2^n \times m}, \quad (10)$$

where  $S_{[T, \frac{5}{2}T]}$  denotes the wavefunction evolved over the (discretized) time interval  $[T, \frac{5}{2}T]$ , where we overlap the



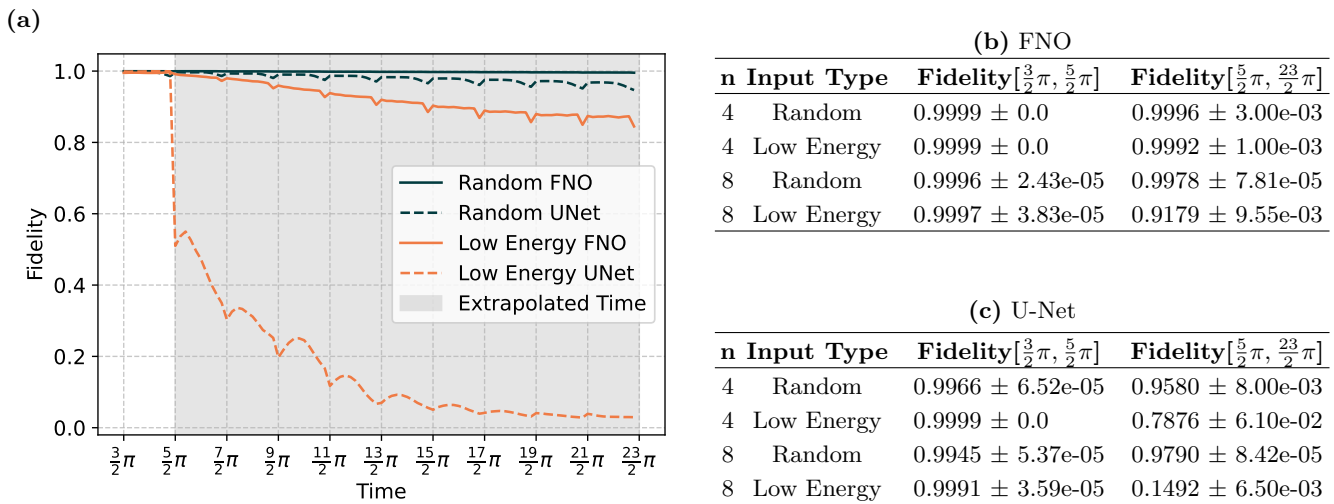


Figure 3: **(a)** Prediction of temporal dynamics in an 8-qubit Heisenberg spin system using the time-domain architecture, with FNO and U-Net. The input time interval is denoted as  $[0, \frac{3}{2}\pi]$ , as illustrated in Figure 1 d), while the extrapolated time refers to future time predictions beyond the trained range. **(b)** The results present the mean fidelity for both the training time (i.e., the time intervals the FNO encountered during training) and the extrapolated time  $[\frac{5}{2}\pi, \frac{23}{2}\pi]$  for systems with 4 and 8 qubits, across different input types. **(c)** The results show the mean fidelity using U-Net for similar inputs and time intervals.

time interval  $[T, \frac{3}{2}T]$  with the one of the input  $\mathbf{I}$  in Eq. (9). This setup facilitates smoother and more accurate learning, as the FNO can leverage the temporal continuity and patterns in the evolved wavefunction data. Consequently, the output includes the future time interval  $[\frac{3}{2}T, \frac{5}{2}T]$ , unseen during training. We use two different sets of previously described inputs, i.e., random wavefunctions and low-energy wavefunctions. While the basis states does not necessarily need to be ordered as in the previous architecture, we maintain the order for consistency.

We also perform extrapolated time prediction by applying the model on its predicted time intervals to predict unseen future time intervals, up to  $t = \frac{23}{2}T$ , as seen in Figure 3. The fidelity metrics for both the training intervals and the extrapolated times are also reported in Figure 3, demonstrating that even with substantial predictions into the future, the FNO achieves exceptionally high fidelities for systems of both 4 and 8 qubits. Additionally, we compare the performance of the FNO with that of a deep neural network, specifically a U-Net [45]. Our evaluation demonstrates that the FNO outperforms the U-Net, especially in the extrapolated time regime, as seen in Figure 3. Moreover, even at moderate system sizes (8 qubits), the FNO achieves a 6.71x speedup compared to the exact unitary-based method in predicting the dynamics of random inputs up to  $t = \frac{23}{2}T$ , with only a negligible fidelity reduction of 0.04%.

Additionally, we performed evaluations on the output time interval  $[T, \frac{5}{2}T]$  using a finer grid with width  $\Delta t = \pi/100$  for a 4-qubit system with random inputs. For the FNO, the resulting fidelity of 0.9999 was iden-

tical to that obtained on the coarser training discretization. While we can also apply the U-Net on the finer grid, it is not discretization-agnostic, leading to an error rate of 4.78% in the expected fidelity. To further demonstrate the FNO’s capability to achieve zero-shot super-resolution, we used an input interval of  $[0, \frac{3}{2}T]$  with  $T = 5\pi$  and  $\Delta t = \pi/2$  for 4 qubits and evaluated the corresponding output interval on a finer grid with  $\Delta t = \pi/20$ . The FNO successfully predicted the finely discretized output with an error rate of just 0.04%, whereas the U-Net demonstrated a significantly higher error rate of 51.70% compared to the coarse grid fidelity.

### C. Learning Dynamics using Hamiltonian Observables

Hamiltonian observables refer to the individual terms (observables) from the time-evolution generator (Hamiltonian) of the quantum wavefunction. These observables are obtained using the wavefunction by calculating the expectation values for the individual observable terms. For example, in the Ising model, the observables could include terms like  $\sigma_z \sigma_z$  or  $\sigma_z$  while in the Heisenberg model, they could include  $\sigma_a \sigma_a$  (where  $a \in \{x, y, z\}$ ) and  $\sigma_z$ . Using observables from the Hamiltonian, instead of the full wavefunction, as inputs and outputs for the FNO greatly enhances its scalability, as there are approximately  $\text{poly}(n)$  terms in the former and  $2^n$  terms in the latter. This compression would allow us to train and make predictions with quantum systems that are too large or long to simulate directly, e.g., by us-

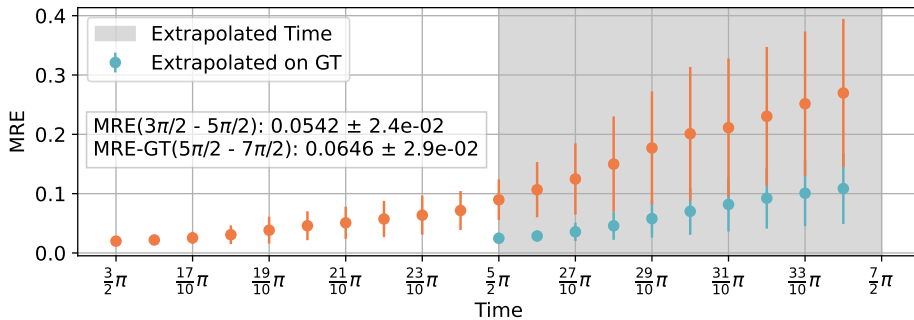


Figure 4: Mean Relative Error (MRE) for predicted Hamiltonian observables in an 8-qubit system using FNO, utilizing the time-domain architecture. The model is trained on the input time interval  $[0, \frac{3}{2}\pi]$  as shown in Figure 1 d) and predicts the output interval  $[\frac{3}{2}\pi, \frac{5}{2}\pi]$ . Additionally, it extrapolates future unseen dynamics  $[\frac{5}{2}\pi, \frac{7}{2}\pi]$ , which is twice the length of the output interval. For extrapolated time predictions on ground truth (GT), the MRE is 6.46%. This is particularly significant in quantum simulations, where the primary objective is to extend these simulations. Additionally, based on the time interval the model was trained on, the MRE for extrapolated time predictions is 11.18% denoted by orange dashes. We additionally calculate the mean MSE loss for the training time interval as  $3.096 \times 10^{-6} \pm 2.497 \times 10^{-6}$  and for future time predictions over the same interval on ground truth as  $4.212 \times 10^{-6} \pm 3.333 \times 10^{-6}$ .

ing data from large quantum devices or wide tensor networks, from which we could then infer times longer than the devices’ coherence time or past the tensor network’s tractable depth, respectively. However, predicting future dynamics based on these partial observables presents a significant challenge, particularly without explicit knowledge of the underlying Hamiltonian.

To evaluate the FNO’s capabilities, we first considered the Ising Hamiltonian as described in Eq. (2), where  $J_z$  and  $h$  are randomly generated. Importantly, in this study, we focus on using random wavefunction states to calculate the expectation values of these observables, making the learning and prediction tasks for the FNO maximally general and, as a result, challenging.

For the observables, we exclusively utilize the time-domain architecture. In this setup, the input consists of predefined observables and their time-evolved intervals. We provide a detailed description of the specific observables used in Section III. This input structure mirrors the previously described input  $\mathbf{I}$  in Eq. (9), but instead of wavefunction basis states  $S$ , it includes observable quantities. This setup presents a substantial challenge for the FNO, as it must learn to predict future dynamics based on only partial information about the quantum state.

We further extrapolate to the future time interval  $[\frac{5}{2}T, \frac{7}{2}T]$ , effectively doubling the dynamics captured within the output time interval  $[\frac{3}{2}T, \frac{5}{2}T]$ . This feature is particularly advantageous for quantum computing, where the limited coherence time of error-corrected qubits imposes constraints on the length of computations. Additionally, it can also be integrated to take observable data from tensor network methods and extrapolate it to timescales that would be computationally difficult for it to calculate due to high tensor train rank. Given

that these observables present challenges for the FNO to learn effectively, we extrapolate future times based on the ground truth of the predicted time interval. This approach helps minimize unnecessary errors, as the ground truth is typically known. As seen in Figure 4, with a system of 8 qubits we predict future observables with a relative error of 6.46%, even when extending the prediction to double the train time horizon on ground truth.

## II. DISCUSSIONS

We have presented two FNO architectures that are capable of not only learning the time-evolutions of quantum systems, but also of extrapolating these evolutions to later times. The energy-domain architecture is more compact, requiring fewer computational inputs, and hones in on key dynamics by prioritizing slow quantum transitions. The time-domain architecture is agnostic to the discretization of the time interval, making it highly versatile for obtaining the output state of quantum evolution at arbitrary times. Both methods demonstrate the ability of FNOs to not only carry out quantum state evolution, but to learn the underlying time-evolution operator itself, which constitutes a key accomplishment in the ubiquitous and challenging task of solving the Schrödinger equation.

Of foremost interest is the application of the time-domain FNO using only Hamiltonian observables as input and output. This difficult learning task requires that the FNO learn and conduct future inference on partial information, using only  $\sim \text{poly}(n)$  expectation values rather than the full  $2^n$ -component wavefunction. Under this architecture, the FNO could feasibly be trained

using measurements from noisy quantum devices or data from shallow tensor networks, then infer to later time-scales that are otherwise out of reach of contemporary techniques as they would require either more coherent quantum computers or intractably large tensor networks.

In subsequent research, such a hybrid implementation of our work should be carried out using a large quantum device and a classical FNO to extrapolate to longer times. As open quantum systems have distinct dynamics from their pure counterparts, FNOs should also be applied to noisy quantum states. Moreover, the impact of physical noise and system symmetry on the requisite FNO dimensions and training data size should be studied. As quantum noise, sampling errors, and symmetries can reduce the learning complexity of the quantum system, it is natural that we characterize the FNO in this capacity.

### III. METHODS

We provide details on the wavefunction ordering protocol used in Section IB 1, the types of Pauli strings utilized in Section IC, and the specifics of the training data, and FNO configurations for Figures 2, 3, and 4.

The quantum wavefunction  $\psi$  of a system with  $n$  qubits is represented as a vector in a  $2^n$ -dimensional Hilbert space. The basis states  $\phi_i$  correspond to different qubit configurations, ordered by their binary representation. To reorder the wavefunction by energy levels, we arrange the basis states such that their associated energies  $E_i$  satisfy  $E_i \leq E_{i+1}$ . The wavefunction is then expressed as,

$$\psi = \sum_{i=1}^{2^n} c_i \phi_i. \quad (11)$$

Here  $\phi_i$  are ordered according to increasing energy lev-

els. The energy levels can be calculated using  $E_i = \langle \phi_i | H | \phi_i \rangle$ , where  $H$  is the Hamiltonian of the system.

In Section IC, for a system of 8 qubits, we use a set of 48 observables that includes all nearest-neighbor interactions  $XX$ ,  $YY$ , and  $ZZ$  interactions across all qubit pairs. Additionally, the set includes single-qubit interactions  $X$ ,  $Y$  and  $Z$ . We focus exclusively on quantities exceeding a certain threshold (e.g., greater than  $10^{-2}$ ) to avoid including less significant values that might inflate the relative error. Given that these observables are the expectation values of Pauli strings, we employ Mean Squared Error (MSE) and Mean Relative Error (MRE) as our loss metrics to evaluate the model's performance.

In Figure 2, an 8-qubit system is used with 4,000 training data points, 4 FNO blocks, and 128 modes retained in the Fourier integral operator after truncation. For low-energy states with VTI, each interval contains 5,000 training data points.

In Figure 3, the model is again trained with 4,000 data points, using 4 layers and retaining 7 modes in the FNO after truncation. The U-Net is also trained on the same amount of data.

In Figure 4, we use 18,000 training data points with 48 Pauli strings for the 8-qubit system, utilizing 4 layers and retaining 7 modes.

### ACKNOWLEDGMENTS

F.S. acknowledges support from the Caltech Summer Undergraduate Fellowship. J.B. acknowledges support from the Wally Baer and Jeri Weiss Postdoctoral Fellowship. A.A.'s work is supported in part by the Bren endowed chair, the ONR (MURI grant N00014-18-12624), and the AI2050 Senior Fellow Program at Schmidt Sciences.

- 
- [1] R. P. Feynman, in *Feynman and computation* (cRc Press, 2018) pp. 133–153.
  - [2] C. Zalka, Efficient simulation of quantum systems by quantum computers, *Fortschritte der Physik: Progress of Physics* **46**, 877 (1998).
  - [3] S. Lloyd, Universal quantum simulators, *Science* **273**, 1073 (1996).
  - [4] I. M. Georgescu, S. Ashhab, and F. Nori, Quantum simulation, *Reviews of Modern Physics* **86**, 153 (2014).
  - [5] A. J. Daley, I. Bloch, C. Kokail, S. Flannigan, N. Pearson, M. Troyer, and P. Zoller, Practical quantum advantage in quantum simulation, *Nature* **607**, 667 (2022).
  - [6] E. Altman, K. R. Brown, G. Carleo, L. D. Carr, E. Demler, C. Chin, B. DeMarco, S. E. Economou, M. A. Eriksson, K.-M. C. Fu, *et al.*, Quantum simulators: Architectures and opportunities, *PRX quantum* **2**, 017003 (2021).
  - [7] S. Ebadi, T. T. Wang, H. Levine, A. Keesling, G. Semeghini, A. Omran, D. Bluvstein, R. Samajdar, H. Pichler, W. W. Ho, *et al.*, Quantum phases of matter on a 256-atom programmable quantum simulator, *Nature* **595**, 227 (2021).
  - [8] F. Tacchino, A. Chiesa, S. Carretta, and D. Gerace, Quantum computers as universal quantum simulators: state-of-the-art and perspectives, *Advanced Quantum Technologies* **3**, 1900052 (2020).
  - [9] R. Trivedi, A. Franco Rubio, and J. I. Cirac, Quantum advantage and stability to errors in analogue quantum simulators, *Nature Communications* **15**, 6507 (2024).
  - [10] A. D. King, A. Nocera, M. M. Rams, J. Dziarmaga, R. Wiersema, W. Bernoudy, J. Raymond, N. Kaushal, N. Heinsdorf, R. Harris, *et al.*, Computational supremacy in quantum simulation, arXiv preprint arXiv:2403.00910



- (2024).
- [11] M. Schlosshauer, Quantum decoherence, *Physics Reports* **831**, 1 (2019).
- [12] J. Preskill, Quantum computing in the NISQ era and beyond, *Quantum* **2**, 79 (2018).
- [13] M. Fellous-Asiani, J. H. Chai, R. S. Whitney, A. Auffèves, and H. K. Ng, Limitations in quantum computing from resource constraints, *PRX Quantum* **2**, 040335 (2021).
- [14] S. R. White, Density matrix formulation for quantum renormalization groups, *Physical review letters* **69**, 2863 (1992).
- [15] U. Schollwöck, The density-matrix renormalization group, *Reviews of modern physics* **77**, 259 (2005).
- [16] R. Orús, Tensor networks for complex quantum systems, *Nature Reviews Physics* **1**, 538 (2019).
- [17] Y. Panagakis, J. Kossaifi, G. G. Chrysos, J. Oldfield, T. Patti, M. A. Nicolaou, A. Anandkumar, and S. Zafeiriou, in *Signal Processing and Machine Learning Theory* (Elsevier, 2024) pp. 1009–1048.
- [18] J. Carrasquilla and R. G. Melko, Machine learning phases of matter, *Nature Physics* **13**, 431 (2017).
- [19] G. Carleo and M. Troyer, Solving the quantum many-body problem with artificial neural networks, *Science* **355**, 602 (2017).
- [20] G. Torlai, G. Mazzola, J. Carrasquilla, M. Troyer, R. Melko, and G. Carleo, Neural-network quantum state tomography, *Nature physics* **14**, 447 (2018).
- [21] H. Lange, A. Van de Walle, A. Abedinnia, and A. Bohrdt, From architectures to applications: A review of neural quantum states, *Quantum Science and Technology* (2024).
- [22] C.-D. Han, B. Glaz, M. Haile, and Y.-C. Lai, Tomography of time-dependent quantum Hamiltonians with machine learning, *Physical Review A* **104**, 062404 (2021).
- [23] N. Mohseni, T. Fösel, L. Guo, C. Navarrete-Benlloch, and F. Marquardt, Deep learning of quantum many-body dynamics via random driving, *Quantum* **6**, 714 (2022).
- [24] Z. Li, N. Kovachki, K. Azizzadenesheli, B. Liu, K. Bhattacharya, A. Stuart, and A. Anandkumar, Fourier neural operator for parametric partial differential equations, arXiv preprint arXiv:2010.08895 (2020).
- [25] J. Kossaifi, N. Kovachki, K. Azizzadenesheli, and A. Anandkumar, Multi-Grid Tensorized Fourier Neural Operator for High-Resolution PDEs, arXiv preprint arXiv:2310.00120 (2023).
- [26] Z. Li, D. Z. Huang, B. Liu, and A. Anandkumar, Fourier neural operator with learned deformations for PDEs on general geometries, *Journal of Machine Learning Research* **24**, 1 (2023).
- [27] L. Lingsch, M. Y. Michelis, E. de Bezenac, S. M. Perera, R. K. Katzschmann, and S. Mishra, Beyond Regular Grids: Fourier-Based Neural Operators on Arbitrary Domains, arXiv preprint arXiv:2305.19663 (2023).
- [28] Z. Li, N. Kovachki, C. Choy, B. Li, J. Kossaifi, S. Otta, M. A. Nabian, M. Stadler, C. Hundt, K. Azizzadenesheli, *et al.*, Geometry-informed neural operator for large-scale 3d PDEs, *Advances in Neural Information Processing Systems* **36** (2024).
- [29] S. Lanthaler, A. M. Stuart, and M. Trautner, Discretization error of Fourier neural operators, arXiv preprint arXiv:2405.02221 (2024).
- [30] H. Maust, Z. Li, Y. Wang, D. Leibovici, O. Bruno, T. Hou, and A. Anandkumar, Fourier continuation for exact derivative computation in physics-informed neural operators, arXiv preprint arXiv:2211.15960 (2022).
- [31] B. Bonev, T. Kurth, C. Hundt, J. Pathak, M. Baust, K. Kashinath, and A. Anandkumar, Spherical Fourier neural operators: learning stable dynamics on the sphere, *Proceedings of the 40th International Conference on Machine Learning (ICML)* **202**, 2806 (2023).
- [32] J. Helwig, X. Zhang, C. Fu, J. Kurtin, S. Wojtowysch, and S. Ji, in *Proceedings of the 40th International Conference on Machine Learning*, ICML'23 (JMLR.org, 2023).
- [33] Z. Li, W. Peng, Z. Yuan, and J. Wang, Fourier neural operator approach to large eddy simulation of three-dimensional turbulence, *Theoretical and Applied Mechanics Letters* **12**, 100389 (2022).
- [34] S. Mizera, Scattering with neural operators, *Physical Review D* **108**, L101701 (2023).
- [35] J. B. Parkinson and D. J. Farnell, *An introduction to quantum spin systems*, Vol. 816 (Springer Science & Business Media, 2010).
- [36] S. Sachdev, Quantum phase transitions, *Physics world* **12**, 33 (1999).
- [37] A. W. Sandvik, in *AIP Conference Proceedings*, Vol. 1297 (American Institute of Physics, 2010) pp. 135–338.
- [38] A. Anandkumar, K. Azizzadenesheli, K. Bhattacharya, N. Kovachki, Z. Li, B. Liu, and A. Stuart, in *ICLR 2020 Workshop on Integration of Deep Neural Models and Differential Equations* (2019).
- [39] B. Raonic, R. Molinaro, T. De Ryck, T. Rohner, F. Bartolucci, R. Alaifari, S. Mishra, and E. de Bézenac, in *Advances in Neural Information Processing Systems*, Vol. 36 (2024).
- [40] N. Kovachki, Z. Li, B. Liu, K. Azizzadenesheli, K. Bhattacharya, A. Stuart, and A. Anandkumar, Neural operator: Learning maps between function spaces with applications to PDEs, *Journal of Machine Learning Research* **24**, 1 (2023).
- [41] K. Azizzadenesheli, N. Kovachki, Z. Li, M. Liu-Schiaffini, J. Kossaifi, and A. Anandkumar, Neural operators for accelerating scientific simulations and design, *Nature Reviews Physics* , 1 (2024).
- [42] S. Lanthaler, Z.-Y. Li, and A. M. Stuart (2023).
- [43] I. N. Levine, D. H. Busch, and H. Shull, *Quantum chemistry*, Vol. 6 (Pearson Prentice Hall Upper Saddle River, NJ, 2009).
- [44] C. Trabelsi, O. Bilaniuk, Y. Zhang, D. Serdyuk, S. Subramanian, J. F. Santos, S. Mehri, N. Rostamzadeh, Y. Bengio, and C. J. Pal, in *International Conference on Learning Representations* (2018).
- [45] C. Williams, F. Falck, G. Deligiannidis, C. C. Holmes, A. Doucet, and S. Syed, A unified framework for U-Net design and analysis, *Advances in Neural Information Processing Systems* **36**, 27745 (2023).